Langmuir

Article

pubs.acs.org/Langmuir

Time-of-Flight Secondary Ion Mass Spectrometry with Principal Component Analysis of Titania–Blood Plasma Interfaces

Ricardo Tejero,[†,‡,⊥] Peggy Rossbach,[§] Beat Keller,[§] Eduardo Anitua,[∥] and Ilya Reviakine*[,‡,⊥]

[†]BTI ImasD, Leonardo da Vinci 14B, 01510 Vitoria, Spain.

[‡]CIC biomaGUNE, Paseo Miramón 182, 20009 San Sebastián, Spain.

[§]EMPA, Ueberlandstraße 129, CH-8600 Dübendorf, Switzerland.

[∥]Private practice in implantology and oral rehabilitation, José Ma Cagigal 19, 01007 Vitoria, Spain

[⊥]Department of Biochemistry and Molecular Biology, University of the Basque Country, 48940 Leioa, Spain

Supporting Information

ABSTRACT: Treatment of osseoimplant surfaces with autologous platelet-rich plasma prepared according to the plasma rich in growth factors (PRGF-Endoret) protocol prior to implantation yields promising results in the clinic. Our objective is to understand the organization of complex interfaces between blood plasma preparations of various compositions and model titania surfaces. Here we present the results of the morphological and chemical characterization of TiO_2 surfaces incubated with four types of blood plasma preparations devoid of leukocytes and red blood cells: either enriched in platelets (PRGF-Endoret) or platelet-depleted, and either activated with $CaCl_2$ to induce clotting, or not. Chemical characterization was done by time-of-flight secondary ion mass spectrometry with principal component analysis (ToF-SIMS/PCA). The interface morphology was studied with scanning electron and atomic force microscopy. Immunofluorescence microscopy was used to identify platelets and infer their activation state. We observe clear differences among the four types of interfaces by ToF-SIMS/PCA. Some of these could be straightforwardly related to the differences in the sample morphology and known effects of platelet activation, but others are more subtle. Strikingly, it was possible to differentiate between these samples by ToF-SIMS/PCA of the protein species alone. This clearly indicates that the composition, orientation, and/or conformation of the proteins in these specimens depend both on the platelets' presence and on their activation. The ToF-SIMS imaging functionality furthermore provides unique insight into the distribution of phospholipid species in these samples.

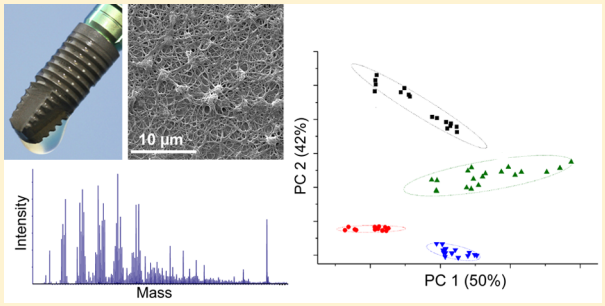

INTRODUCTION

Titanium has been the workhorse of osseoimplantation since the discovery of strong bone–titanium adhesion by Branemark in the 1950s.[1,2] The success of titanium in implantology is to a large extent due to the inertness of its oxide film.[2−4] In fact, the very definition of biocompatibility has been centered around the material inertness—resistance to corrosion, lack of mechanical wear and tear, and minimal immune response.[2]

In recent years, the focus of biocompatibility research has shifted from improving the passive biocompatibility of the kind offered by titanium oxide to designing implants that actively interact with the surrounding tissue, promoting an integrative and regenerative response.[5] To this end, success has been reported with the activation of implant surfaces and implantation sites by incubating them with autologous platelet-rich plasmas immediately prior to implantation (Figure 1).[6−9] We focus in this study on the particular platelet-rich plasma preparation protocol described by Anitua et al.[7,10] This protocol is commercially available under the trade name PRGF-Endoret. Briefly, it entails obtaining leukocyte-free, platelet-rich plasma (2- to 3-fold platelet enrichment factor) from whole blood by one-step centrifugation, activating it with $CaCl_2$ to initiate coagulation and applying the preparation to the surface of the implant as well as to the implantation site immediately before implant placement (shown in translucent yellow in Figure 1).

Natural coagulation pathways activated by the addition of $CaCl_2$ lead to the formation of a biodegradable fibrin network with trapped platelets on the implant surface and at the implantation site; its structure is illustrated in Figure 1c. It is in fact very similar to an incompletely formed blood clot but lacks red and white blood cells. One of the natural functions of clots in the body is to initiate wound healing and regeneration after bleeding stops.[11] These processes are initiated and orchestrated by platelets that release a variety of growth factors upon activation.[11,12] It is therefore expected that platelet accumulation at the implant surface and implantation site (Figure 1) would provide a source of mediators promoting site

Received: March 9, 2012
Revised: October 5, 2012
Published: October 23, 2012

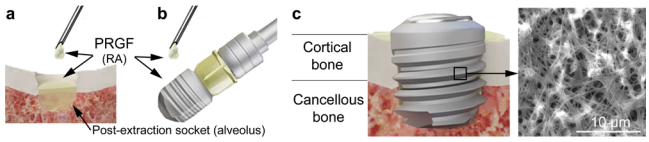

Figure 1. Endosseous dental implant surface activation and placement. (a) Site preparation. The alveolus is cleared of blood and debris (not shown) and filled with plasma rich in growth factors (PRGF-Endoret; translucent yellowish liquid) that has been previously activated with calcium chloride solution. (b) Prior to implantation, the titanium screw to be implanted is wetted with the PRGF-Endoret activated in the same way as on the alveolus. (c) Insertion. The treated implant is placed into the insertion site. The total time elapsed from PRGF-Endoret activation to the end of the implant placement is ∼5−10 min. The implant can be immediately loaded or allowed to heal for some weeks (delayed loading). The use of PRGF-Endoret has been reported to accelerate endosseous implant integration[9,18,19] and reduce the risk of periimplantitis,[55] which may lead to implant failure.

vascularization, mesenchymal stem cell differentiation into osteoblasts and their proliferation, and bone formation.[12−15] Consistent with this idea, PRGF treatment was shown to improve the osseointegration of titanium implants significantly.[7,9,12,16−19] Furthermore, this protocol has been adapted to other biomedical fields and provides significant clinical benefits in terms of wound healing and tissue regeneration. (See ref 20 for a recent review.)

For these reasons, we initiated a program of studies aimed at a careful and systematic physicochemical, biophysical, and biological characterization of biomaterial interfaces treated with various blood-derived preparations. The focus of this particular study is on the chemistry and morphology of model implant surfaces incubated with various blood plasma preparations (Figure 2); biological effects and growth factor release kinetics are presented elsewhere.[21] The question we are addressing is whether we can chemically distinguish the interfaces prepared from blood plasma in different ways and whether these chemical differences can be related to the morphological properties of the interfaces. The chemical composition of the interfaces is analyzed by time-of-flight secondary ion mass spectrometry (ToF-SIMS) with principal component analysis (PCA).[22−24] Complementary information is provided by atomic force microscopy, scanning electron microscopy, and immunostaining fluorescence microscopy.

ToF-SIMS provides chemical information about the top ∼1−3 nm of the surface by bombarding it with ions or ion clusters and by analyzing the molecular fragments knocked out of the surface by time-of-flight mass spectrometry. This technique can therefore provide molecular information,[22,23,25] as opposed to other powerful surface analysis techniques such as X-ray photoelectron spectroscopy (XPS) that yields surface elemental and local chemical compositions. However, ToF-SIMS can lead to rather complex fragmentation patterns that, in the case of proteins, are dominated by fragments smaller than 200 amu. These patterns can be analyzed by principal component analysis (PCA) to obtain information about the protein composition and/or orientation at the interface.[22,23,26] The combination of ToF-SIMS and PCA has been successfully used to study a wide variety of biological specimens at interfaces, from adsorbed single proteins to complex protein mixtures including blood plasma and serum, lipid membranes, and whole cells.[22,23,26−33] We apply it to examine the effects that the platelet content and the activation of the clotting cascade have on the TiO_2−blood plasma interfaces.

MATERIALS AND METHODS

Unless otherwise stated, all reagents were purchased from Scharlab S.L., Spain. The Nanopure water used in this study was obtained by purification with a Diamond UV water system (Branstead International, Iowa, USA).

Blood Plasma Preparation. Blood from healthy volunteers was collected in 3.8% (w/v) sodium citrate-containing tubes (Biotechnology Institute S.L., Spain). Blood samples were centrifuged at 580*g* for 8 min in a PRGF System IV centrifuge (Biotechnology Institute S.L., Spain) to obtain platelet-rich plasma (R) in accordance with the PRGF-Endoret procedure.[17] Platelet-poor plasma (P) was obtained by a second centrifugation at 4500*g* for 12 min at room temperature in a Sigma 3K30 centrifuge (Sartorius AG, Germany). Cell counts were obtained with an ABC Micros60 hematologic counter (Horiba, Japan). They are listed in Table 1.

Surface Preparation and Cleaning. Surfaces used in this study were prepared by coating silicon wafers (University Wafer, Boston, MA, USA) or glass no. 1 25-mm-round microscope coverslips (Menzel-Gläser, Braunschweig, Germany) with an ∼20 nm thick layer of TiO_2 by magnetron reactive sputtering according to the procedure described in Kurrat et al.[34] The coating was done at the Paul Scherrer Institute (PSI, Villigen, Switzerland). Coated wafers were cut into 1 × 1 cm^2 plates before use.

Immediately prior to each experiment, surfaces were cleaned. First, samples were sonicated in a 2% sodium dodecyl sulfate (Fluka Analytical, Sigma-Aldrich GmbH, Germany) solution that was filtered through a 0.2-μm-pore-diameter syringe filter (Millipore, Billerica, MA, USA) and rinsed under stream of Nanopure water. Water was blown off with a filtered nitrogen stream. Dry surfaces were further treated with UV−ozone for 30 min in a UV−ozone cleaner (BioForce Nanosciences, USA) that was preheated for 30 min immediately before use.

The chemical composition of the surfaces before and after cleaning was confirmed by XPS analysis with a SAGE HR100 instrument (Specs, Berlin, Germany) with a nonmonochromated Mg Kα source operating at 300 W. A pass energy of 30 eV was used for survey scans, and 15 eV was used for detailed scans. Spectra were calibrated using the C 1s peak at 285.0 eV and analyzed using CasaXPS software (Casa Software Ltd.). Surfaces used in this study contained ∼12 atomic % carbon and typically contained more than 95% TiO_2 (as opposed to the lower oxides, TiO or Ti_2O_3). A representative XPS spectrum is shown in Figure S1 and Table S1 in the Supporting Information. Further information about the surface analysis of titania films can also be found in Sittig et al.,[35] Textor et al.,[36] and Callen et al.[37]

Preparation of Samples for ToF-SIMS Analysis. Freshly cleaned surfaces were coated with 20 μL of the appropriate plasma preparation (R or P). For the activated versions (RA and PA, respectively), 10 wt % calcium chloride hexahydrate solution (Biotechnology Institute S.L., Spain) was applied to the surfaces before application of the plasma. The preparation of the four samples is shown in Figure 2b,c. The final concentration of $CaCl_2$ in the plasma was 22.8 mM. After an incubation time of 10 min, surfaces were gently rinsed with Nanopure water and stored for 8 h before ToF-SIMS analysis.

Time-of-Flight Secondary Ion Mass Spectrometry (ToF-SIMS) and Principal Component Analysis (PCA) of ToF-SIMS Data. Static ToF-SIMS measurements were performed in a TOF-SIMS V instrument from Ion-ToF GmbH (Munster, Germany) using Bi_3^{2+} primary ions at 50 kV energy and ∼0.3 pA current. The area analyzed was 200 × 200 μm^2, and the primary ion dose was 10^{12} ions/cm^2. Both positive and negative secondary ions were analyzed. The mass resolution ($m/\Delta m$) was typically above 4000 for all of the peaks studied. Low-energy electron flooding in order to reduce sample charging was unnecessary except for one measurement, which was excluded from further analysis. The measurements were made at about 4 × 10^{-9} mbar at room temperature.

Before further analysis, spectra were calibrated with Ion-Tof Ion Spectra software (version 6.2, Ion-Tof, GmbH, Munster, Germany) using CH_3^+, $C_2H_3^+$, $C_3H_7^+$, $C_5H_3^+$, $C_7H_7^+$, $C_9H_{12}^+$, C^-, CH^-, C_2^-, C_3^-,

dx.doi.org/10.1021/la303360f | Langmuir 2013, 29, 902−912

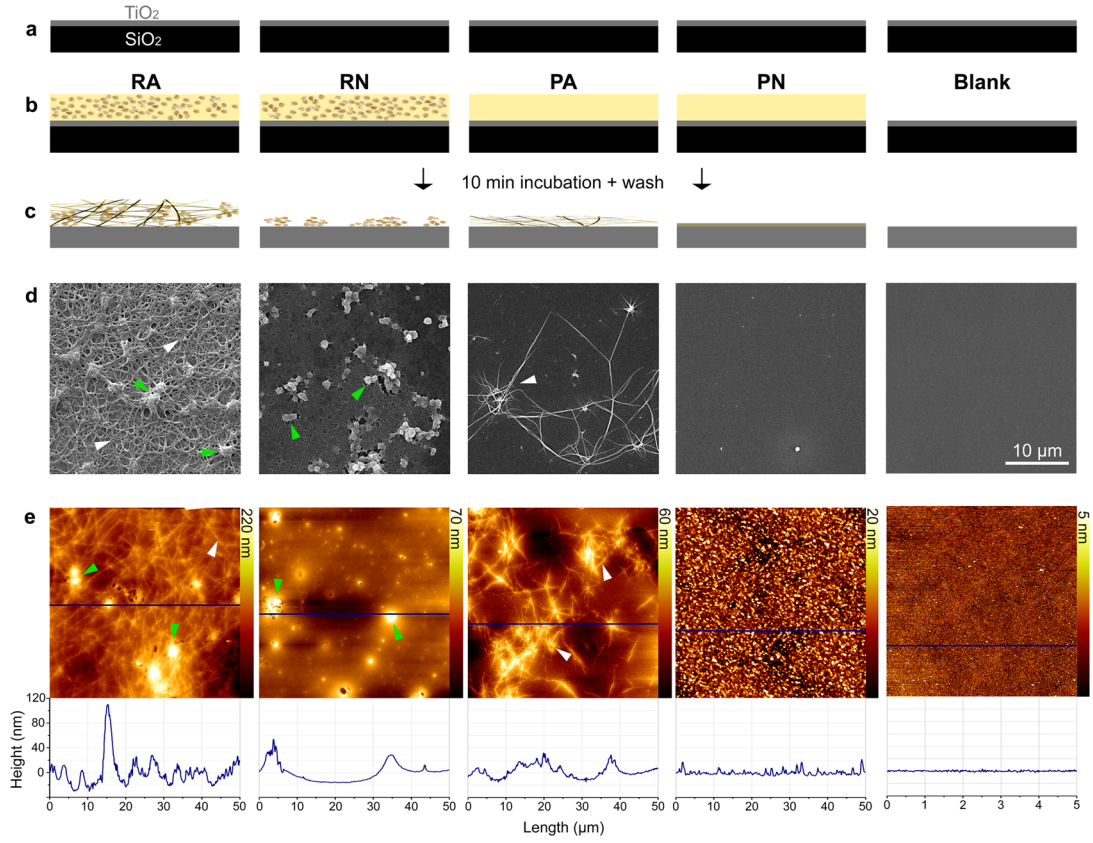

Figure 2. Sample preparation and morphological analysis. (a) Surfaces used in this study consisted of a 15−20 nm TiO_2 layer (gray) prepared on the surface of glass slides or silicon wafers by magnetron reactive sputtering. (b) Appropriate plasma solutions (plasma rich in growth factors or platelet-poor plasma, activated or nonactivated) were deposited onto freshly cleaned surfaces. Activation consisted of the addition of $CaCl_2$ to a final concentration of 22.8 mM. Samples were incubated for 10 min and washed. (c) The preparation procedure results in four types of schematically illustrated samples: RA contains a fibrin network with trapped (activated) platelets; RN contains intact platelets and almost no fibrin; PA contains some fibrin; and PN is essentially a layer of surface-adsorbed proteins. Analyses of these samples by scanning electron microscopy (SEM) and atomic force microscopy (AFM) shown in parts d and e, respectively, confirm the validity of these schematic illustrations. (d) Scanning electron microscopy images of the four types of samples used in this study. Individual platelets and a dense fibrin network are clearly visible in the RA samples, but only platelets can be seen in the RN ones. Because of the absence of Ca^{2+}, the thrombin-generated catalytic cascade is not active here. PA samples contain a small number of fibrin fibrils, most likely due to the presence of a small number of platelets activated upon addition of Ca^{2+} that catalyzed thrombin generation. PN samples are more or less featureless. Green arrows mark platelets and platelet aggregates, and white arrows mark fibrin. (e) Atomic force microscopy images of the four types of samples are seen to correlate with the SEM shown in part d. Platelets and fibrin network, platelets alone, and the residual fibrin network are again visible in the RA, RN, and PA samples, respectively. The PN sample is roughly featureless. Please note that the *z* scale, indicated on the right of each image, is different between images because of the very different morphologies of each interface. The image width is 50 μm. Green arrows mark platelets and platelet aggregates, and white arrows mark fibrin. Height profiles were obtained after the projection of the vertical information along the blue line in the AFM images. As anticipated from the *z*-scale differences, the maximum height variation found in RA surfaces is 2 times that of RN and almost 3 times that of PA. PN samples are comparatively flat. The RA cross section shows that the 3D structure of clots with embedded platelets can be translated to the surface of titania.

and PO_2^- ion peaks, respectively, following the guidelines of Green et al.[38] The same software was used for peak selection.

The statistical analysis of ToF-SIMS data proceeded following Wagner et al.[23] The first step was to select the peaks to be used in the analysis. Peak selection was based on previous studies.[39−41] Selected positive ion peaks corresponding to substrate/Ca, protein fragments, and phospholipids are listed respectively in Tables S2−S4 in the Supporting Information, and selected negative ion peaks corresponding to protein fragments and phospholipids are listed in Table S5 in the Supporting Information.

The area under each peak was computed identically for all spectra and samples and normalized by the total ion counts in all of the selected peaks from the given sample in order to factor out topographic and matrix effects.[22] Before statistical analysis, all peak intensities were mean-centered so that the origin-centered data set variance was due to differences in sample variance rather than differences in sample means.

At this point, each kind of sample (RA, RN, PA, and PN) was described by 16 sets of peak intensities (the lists of peaks are shown in Tables S2−S5). These 16 sets originated from two replicas of each kind of sample. For each replica, data was collected from two different 200 × 200 μm^2 areas on the sample that were split into 50 × 50 μm^2 areas for analysis. Principal component analysis (PCA) was performed on these sets of intensities in a NESAC/BIO Toolbox[42] in Matlab (Mathworks Inc., USA). PCA assigns to each set a point in space defined by the principal components. Sets originating from identically prepared samples cluster together. To determine the limits of the 95% confidence intervals around each such cluster, a procedure described in Wagner et al.[23] was followed. It consisted of performing a second PCA on the mean-centered subset of scores of the sample types whose statistical limits were being determined. The eigenvalues of this second PCA are the major and minor axes of an ellipse that can be drawn around the scores. The ellipse represents the confidence limits of the subset of scores in the second PCA. The loadings of the second PCA

dx.doi.org/10.1021/la303360f | *Langmuir* 2013, 29, 902−912

Table 1. Leukocyte, Erythrocyte, and Platelet Counts of the Plasma Solutions Used in the ToF-SIMS, AFM, FM, and SEM Experiments[a]

experiment	plasma preparation	leukocytes × $10^3/\mu L$	erythrocytes × $10^6/\mu L$	platelets × $10^3/\mu L$ (enrichment factor)
ToF-SIMS	R	0.00	0.03	620 (2.16)
	P	0.00	0.01	22 (0.08)
AFM	R	0.10	0.02	420 (2.80)
	P	0.10	0.00	4 (0.03)
FM	R	0.10	0.01	380 (1.90)
	P	0.00	0.00	12 (0.06)
SEM	R	0.00	0.00	404 (2.08)
	P	0.10	0.00	1 (0.01)
avg ± SD[a]	R	0.05 ± 0.06	0.00 ± 0.01	456 ± 111 (2.24 ± 0.39)
	P	0.05 ± 0.06	0.02 ± 0.01	9.75 ± 9.4 (0.05 ± 0.05)

[a]This row shows the average values ± std dev. The platelet enrichment factor shown is relative to the platelet concentration in whole blood. R refers to platelet-rich (PRGF-Endoret) preparations; P refers to the platelet-poor ones.

can be then used to rotate the ellipse from the secondary PCs so that it corresponds to the original PC plot.

Scanning Electron Microscopy (SEM). Scanning electron microscopy (SEM) analysis was performed with a Hitachi S-4800 (Hitachi, Japan) at 15 kV acceleration voltage at around a 10 mm working distance. Representative images at 2000× and 3000× were cropped to a 30 × 30 μm^2 size.

Samples prepared identically as for ToF-SIMS analysis were fixed for 1 h in 2 wt % glutaraldehyde in 0.1 M sodium cacodylate buffer (pH 7.4) at room temperature, washed 3 × 10 min with the 6.5 wt % sucrose in the same cacodylate buffer, stained with 1 wt % OsO_4 in 0.1 M cacodylate buffer for 1 h at 4 °C in the dark, and finally washed 3 × 10 min with cacodylate buffer. Fixed samples were dehydrated in a series of solutions of increasing ethanol concentrations (30, 50, 70, 96, 3 × 100 vol %). Each step took 10 min. Dehydrated samples were immersed in hexamethyldisilazane for 2 × 10 min and allowed to dry. Dry samples were coated with gold by sputtering for 180 s immediately before observation in an argon atmosphere in a JFC-1000 ion sputterer (Jeol Ltd., Japan) mounted on one of the ports of the SEM. Detailed descriptions of these protocols can be found in refs 43−45.

Fluorescence Microscopy (FM). Fluorescence microscopy was carried out in a Zeiss LSM 510 scanning laser confocal fluorescence microscope using a 63× oil immersion objective and laser lines and filters appropriate for each die. Clean TiO_2-coated glass coverslips were placed in a homemade Teflon holder and incubated with 100 μL of the appropriate plasma solution (RA, RN, PA, and PN) for 10 min before washing and examination. Immunostaining for quiescent and activated platelets was done by incubating plasma samples for 1 h before substrate coating with fluorescently labeled mouse-antihuman antibodies against CD42a and CD62P, respectively (BD Biosciences, Franklin Lakes, NJ, USA). Antibodies were diluted 1:25 prior to use.

Atomic Force Microscopy (AFM). Samples used in the AFM experiments were prepared in the same way as those used in the ToF-SIMS analysis. AFM imaging of the topography was performed with a JPK Nanowizard II atomic force microscope (JPK Instruments AG, Germany). AFM images were collected in tapping mode in air. Oxide-sharpened silicon nitride tips mounted on V-shaped cantilevers with a nominal spring constant of 0.32 N/m were used to obtain the images. Height trace images were flattened and plane fitted as required in the JPK image processing software. This software was also used for the measurement of the fibril diameters and the roughness calculations of line profiles.

RESULTS AND DISCUSSION

In this work, we studied the morphology and the chemical composition of four different blood plasma preparations on TiO_2 surfaces: plasma rich in growth factors or platelet-poor plasma, activated with Ca^{2+} or not activated (designated RA, RN, PA, and PN in Figure 2 and throughout the text). The compositions of the different plasma preparations used in these experiments are listed in Table 1. One of these—activated plasma rich in growth factor preparation, RA—emulates titanium implant activation with autologous platelet-rich plasma introduced in the clinic by Anitua and colleagues to enhance the integration of dental implants (Figure 1).[7−9] As expected, these interfaces are morphologically and chemically complex. The key finding of our study is that we were able to detect subtle differences between these interfaces.

Interface Morphology. TiO_2 surfaces incubated with blood plasma present markedly different morphologies depending on the presence or absence of platelets and on whether the samples were treated with Ca to activate platelets and initiate clotting (Figure 2d,e). Activated platelets catalyze the production of thrombin at their surfaces, which in turn catalyzes the formation of the fibrin network from fibrinogen. Indeed, it is evident in Figure 2d,e that a dense network of fibrils connecting circular objects of ∼2−4 μm in diameter is present in the platelet-containing, Ca-activated plasma samples (RA). This is the typical appearance of a clot—fibrin matrix interconnecting platelets.[46] However, only platelets, without the fibrin network, were found in the RN samples. Platelets found in the RN samples were smaller (∼ 1 to 2 μm diameter) than those found in RA samples. This difference is consistent with what is known about platelet morphological changes upon activation: a large amount of surface area stored in the open canalicular system in the quiescent platelets becomes available upon activation, leading to a size increase.[47] Somewhat surprisingly, in RN samples, platelets were found in aggregates. Very few platelets were found in the platelet-poor (PN) preparations. Some fibrils were observed in the activated PA samples, whereas only a featureless film of material—most likely adsorbed plasma proteins—was found on the surfaces of PN samples.

More information could be obtained from the AFM images. In particular, the cross sections shown in Figure 2e are indicative of the topographical heterogeneity of the samples: in RA, platelets and the fibrin network were interspersed with numerous interstitial spaces, leading to a very heterogeneous interface and a height variation of ∼150 nm (peak-to-valley roughness, R_t). The corresponding root-mean-square roughness R_q was 23 nm. The surfaces of the platelet-rich, nonactivated samples were much more homogeneous topographically, with the platelets protruding above the protein film (R_t = 70 nm, R_q = 15 nm). PA samples once again showed topographical heterogeneity derived from the presence of loose and unconnected fibrils (R_t = 50 nm and R_q = 10 nm). Finally, PN samples were very homogeneous, given that they lack both platelets and a fibrin network. The profile of the PN samples was rather flat, with $R_t \approx 20$ nm and $R_q \approx 4$ nm. For comparison, the roughness values of the bare samples were ∼10 nm (R_t) and 0.9 nm (R_q).

The fibril networks found in RA and PA samples were different in terms of the density, length, and thickness of the fibrils. The difference in thickness was not dramatic: fibrils in RA were 217 ± 29 nm wide, and in PA they were 189 ± 35 nm.

dx.doi.org/10.1021/la303360f | Langmuir 2013, 29, 902−912

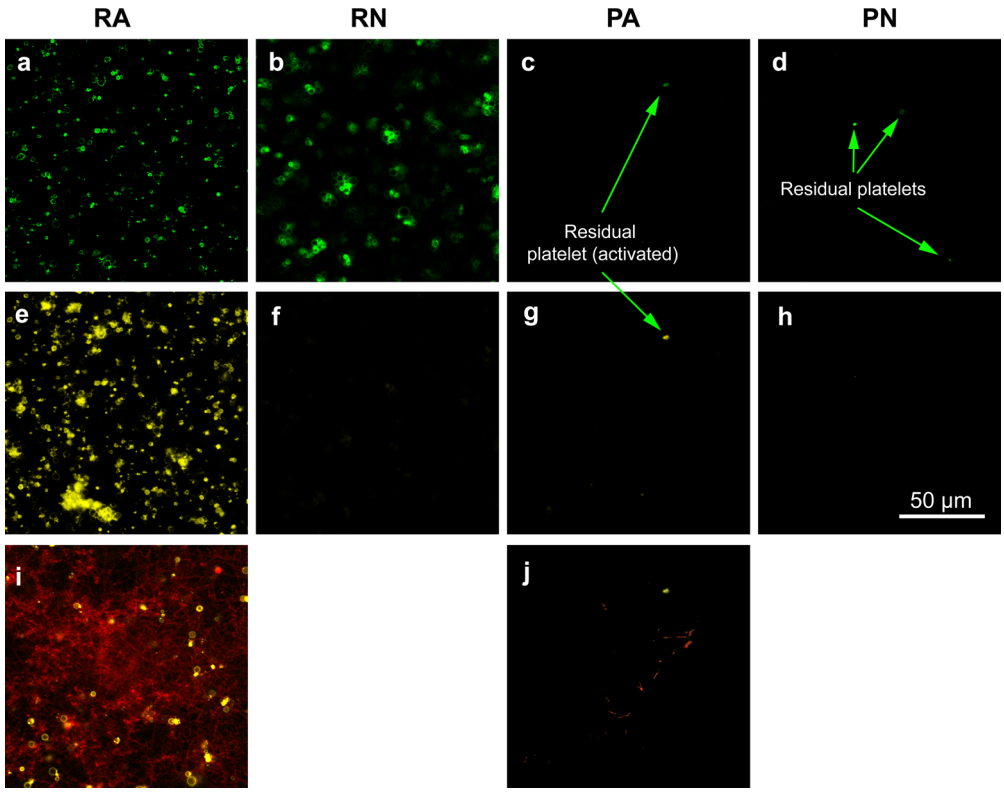

Figure 3. Immunofluorescence microscopy characterization of the blood-plasma-coated TiO_2 surfaces. (a) Platelet identification was performed by staining the samples with the anti-CD42b antibody (green). Platelet activation was assayed by staining them with the anti-CD62P antibody (yellow). Platelets are present in RN preparations (positive staining with CD42b, a and b) but are (nearly) absent from the PN preparations (c and d). Positive anti-CD62P staining indicates that platelets in the Ca-activated preparations are activated (e and g), as expected. A dense network of fibrils is visible by autofluorescence in the RA preparation (red, i), and some fibrils are also visible in the PA preparation (j), consistent with the AFM and SEM images. (a, e, i) RA, (b, f) RN, (c, g, j) PA, and (d, h) PN.

Both values are within the range expected for human fibrin fibrils (~150−350 nm).[46] The fibrils in RA samples were significantly longer and formed denser networks, consistent with the notion that platelets organize the fibrin network and catalyze its production.[47,48]

Neither SEM nor AFM provides chemical or biological information about the film composition. Therefore, the morphological identification of platelets made above was confirmed by immunofluorescence microscopy. Images taken before and after washing were identical, so only the images taken after washing are shown (Figure 3). The globular structures thought to be platelets indeed stained positive for platelet-specific anti-CD42b antibody (Figure 3a−d) and in the case of the activated platelets, for anti-CD62P antibody (Figure 3e−h). CD62P (P-selectin) is a transmembrane protein that is absent from the surface of the inactive platelets but is expressed after activation.[47] These immunofluorescence results confirm that the platelets in RN preparations are in fact not activated in the sense that they do not express α-granule marker CD62P, even though they are to some extent aggregated.

Immunofluorescence experiments also confirmed that platelets were nearly absent from the PN preparations (Figure 3c,d,g,h). The presence of platelets in the activated preparation coincided with the formation of the dense fibrin network (Figure 3i,j), which was visible because of the autofluorescence of the fibrin fibers. Autofluorescence in tissues is thought to be due to cross-links formed between structural proteins, and there are other examples of sharp autofluorescence images (e.g., obtained from collagen and elastin[49]).

The presence of fibrils in the PA samples (Figures 2d,e and 3j) merits some discussion. It indicates that some thrombin is present in these samples. This can arise from the activation of the residual platelets present in the PA samples or from thrombin introduced during blood collection or sample preparation procedures. However, the thrombin-catalyzed fibrinogen-to-fibrin conversion step is itself not Ca^{2+}-dependent. Fibrin networks have been observed in fibrinogen/thrombin preparations in the absence of Ca^{2+}.[50] If small amounts of thrombin were produced in our samples during blood collection or at other stages of sample preparation, then we would have seen fibrils in all of our samples, not only in PA and RA. We therefore conclude that residual platelets present in PA samples are responsible for thrombin production and fibril formation in PA samples.

Interface Chemical Composition by ToF-SIMS and Principal Component Analysis (PCA). Typical ToF-SIMS (positive ion) spectra of the bare TiO_2 surface and the TiO_2 surface exposed to the blood plasma preparation (in this case, RA) are shown in Figure 4a,b, respectively. The bare substrate spectrum is quite simple, containing Ti^+ (m/z 48 and isotopes) and TiO^+ (m/z 64 and isotopes) species (Table S2 in Supporting Information) as well as numerous much smaller peaks due to hydrocarbon (C_xH_y) and silicon contamination (Figure 4a). On the contrary, the RA spectrum is rather complex with numerous peaks corresponding to the amino acid and phospholipid fragments (Figure 4b; cf., Tables S3 and S4 in the Supporting Information). The substrate-related peaks are also detectable in this case but are much less intense. In such

dx.doi.org/10.1021/la303360f | Langmuir 2013, 29, 902−912

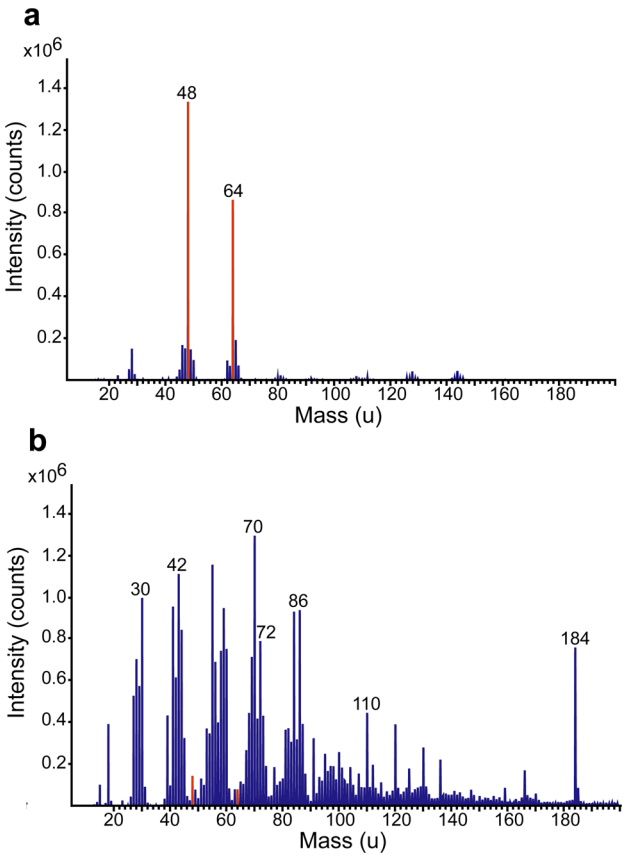

Figure 4. ToF-SIMS analysis of the samples: raw data. (a) Positive ion spectrum of a bare TiO_2 surface before exposure to blood plasma. Ti (m/z 48) and TiO (m/z 64) ions are visible (highlighted in red), as are numerous, less-intense peaks corresponding to adventitious hydrocarbon contamination of the surface. (b) Representative positive ion spectrum of the RA sample. Numerous amino acid fragment peaks are visible, for example, $C_2H_4N^+$ (m/z 42), $C_4H_8N^+$ (m/z 70), and $C_5H_8N_3^+$ (m/z 110), as are the peaks shared by fragments of amino acids and phospholipids (CH_4N^+ (m/z 30), $C_4H_{10}N^+$ (m/z 72) and $C_5H_{12}N^+$ (m/z 86)) and the peak fragment relative to phospholipids only ($C_5H_{15}PNO_4^+$ (m/z 184)).

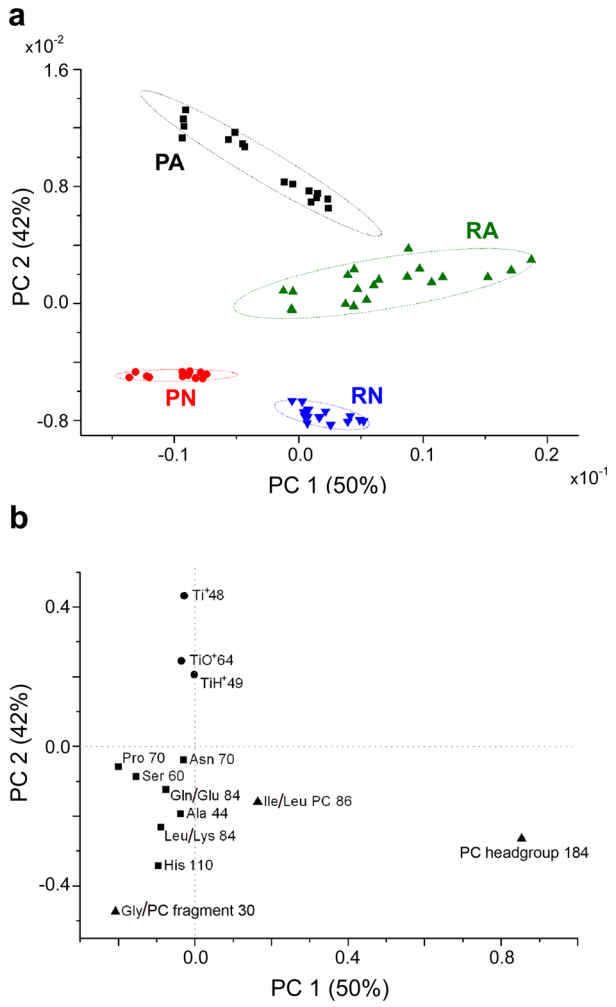

Figure 5. Principal component analysis of the ToF-SIMS data: positive ions. (a) Each point in the space defined by principal components PC1 and PC2 corresponds to a positive ion spectrum in which peaks listed in Tables S2–S4 in the Supporting Information were included. Spectra acquired from identical samples cluster together. The size of each cluster (delineated by the 95% confidence limit ellipsoids) corresponds to the noise within the data—variations in sample preparation and so forth. Clusters corresponding to the different kinds of samples—RA (green), RN (blue), PA (black), and PN (red)—are well separated on this plot. The within-group scatter of –A samples is greater than that of –N samples, indicative of a higher film heterogeneity. (b) Contributions of the individual peaks to each of the two principal components shown in part a are called loadings, and they are plotted in this figure. The main contributions to separation come from three families of peaks: those related to the phospholipids (m/z 30, 86, and 184), to the titania substrate (m/z 48, 49, and 64), and to the amino acid fragments (especially m/z 60, 70, and 110). For clarity, only the high-loading ions are plotted.

complex spectra, the information is encoded in the intensity distribution of various peaks and can be extracted with principal component analysis (PCA) that analyzes similarities and variances between individual sets of intensities (spectra). Each such spectrum becomes a point in space spanned by the principal components, or PCs. Spectra from similar specimens are expected to cluster together (have similar coordinates in the PC space) and separately from the spectra from different kinds of samples. This is indeed what is observed in Figures 5–7, where the results of the three different PCA models of the blood-plasma-treated TiO_2 surfaces are presented. These figures constitute the central result in this article. They show that the four different types of samples—RA, RN, PA, and PN—can be distinguished from each other with respect to the chemical groups accessible to ToF-SIMS (typically, 1–3 nm of the surface layer[22,51]). In other words, these four types of specimens present interfaces that are chemically distinct. We now discuss the origins of these differences.

The model shown in Figure 5a is based on the positive ion peaks corresponding to the substrate (Table S2 in the Supporting Information), protein fragments (Table S3 in the Supporting Information), and phospholipid fragments (Table S4 in the Supporting Information). The selection of peaks used in the classification was based on the previous ToF-SIMS work on the protein and lipid films.[23,31,39,41] The loadings plots (e.g., Figure 5b) indicate how significantly individual chemical species contribute to the separation between the different clusters (sample types) visible in the model (Figure 5a). Specifically, the loadings plot in Figure 5b shows that the substrate species contribute strongly to the separation between the activated and nonactivated samples whereas the phospholipid fragments contribute to the separation between the plasma

dx.doi.org/10.1021/la303360f | Langmuir 2013, 29, 902–912

rich in growth factors versus the platelet-poor plasma samples. The contribution of the phospholipid peaks is straightforward: platelets are the major source of phospholipids in the plasma rich in growth factors devoid of other cells. However, the appearance of the substrate peaks in the activated samples, together with the significantly greater data spread observed in the activated samples (compare the sizes of the ellipses for the PA and RA samples with those for the PN and RN samples in Figure 5a), is indicative of interface heterogeneity, as already noted in the SEM and AFM images (Figure 2). Furthermore, there is a considerable degree of overlap between PA and RA samples along PC1. The reason behind this is not altogether clear, but it is probably related, on one hand, to the retention of the platelets on the surface by the activated samples and, on the other hand, to the heterogeneity of the activated samples already discussed. In our recent study of growth factor release kinetics from TiO_2–blood plasma interfaces of different compositions, we have shown that activated samples on average retain platelets better than nonactivated ones.[21]

The accessibility of the substrate in the Ca-activated samples may be of interest from a clinical point of view. However, it also represents a convolution of interface morphology and chemistry. To investigate further the differences in the interfacial chemistry among these four types of samples, another model was constructed in which only the peaks related to amino acid fragments were considered (Table S3 in the Supporting Information minus peaks with m/z values of 30, 72, and 86). This model should capture the differences related only to the protein composition of the interface. The results of the PCA based on this model are shown in Figure 6. There is clear separation between activated and nonactivated samples, accounting for 69% of the variance of the system; the separation between RN and PN samples is also quite strong (Figure 6a). This is most likely due to the contribution from the platelet proteome in the R-derived samples, although further studies are clearly needed to unravel the sources of these differences.

Interestingly, activation diminishes differences with respect to the protein composition between samples with high and low platelet contents. At this point, we can only speculate on the mechanisms behind this observation: first, activation leads to (partial) loss of the platelet-specific components from the RA samples, making them look more like the PA samples in terms of protein composition. This loss may occur, for example, through the excretion of granule contents[47,52,53] (recall that the samples are washed before the ToF-SIMS analysis, so most of the material released by the platelets was probably lost). Second, AFM and SEM images show that both sets of activated samples (RA and PA) contain fibrin networks. (See the SEM and AFM images of the RA and PA samples in Figure 2.) Nonactivated samples do not. (See the SEM and AFM images of the RN and PN samples in Figure 2.) It appears that the presence of fibrils in the activated samples distinguishes them chemically from the nonactivated ones more than the platelet content distinguishes the activated samples from each other. In other words, fibrin network formation strongly affects interface chemistry. From the loadings plot (Figure 6b), it can be noted that there is a higher relative presence of histidine (His m/z 110) and leucine or lysine (Leu/Lys m/z 84) in nonactivated samples. Raw data (not shown) of PN samples shows a higher relative content on serine (Ser m/z 60) and tryptophan (Trp m/z 130).

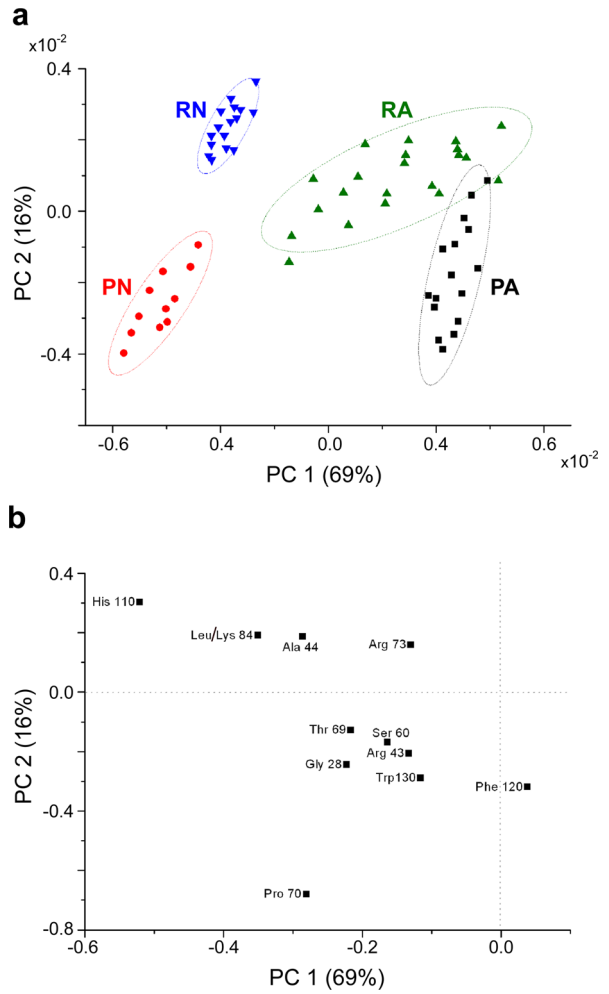

Figure 6. Focus on the proteins: PCA analysis of protein-only peaks from the ToF-SIMS spectra. (a) Same as for Figure 5a, but only the peaks corresponding to the protein fragments listed in Table S3 in the Supporting Information were used. Activated and nonactivated samples are well separated along PC1. Note the much-less-defined separation between RA and PA, whereas the separation between RN and PN is maintained. (b) Loadings plot corresponding to the PCA results shown in part a. Clustering is due to the differences in the relative presence of m/z 70, 84, 110, and 120 for each sample type. For clarity, only the high-loading ions are plotted.

In summary, the presence or absence of platelets and activation translate into differences in protein composition, conformation, and/or orientation in these interfaces.

The negative secondary ions collected by the ToF-SIMS detector are usually largely fragmented and mostly consist of the polyamide backbone-derived groups. In Table S5 in the Supporting Information, we list the selection of relevant negative residues that have been used to build the PCA model shown in Figure 7. It is not surprising that this model less clearly resolves the differences among the samples. However, clustering can still be ascribed to the different sample types (Figure 7a). In the case of negative ions, activation is once again responsible for 69% of the variance whereas differences due to the initial composition (platelets or no platelets) account for only 22%. As already discussed above, activation is related to the changes in protein orientation, conformation, and/or composition at the interface and is accounted for (in the case of the negative ion spectra) in terms of differences in the peaks

dx.doi.org/10.1021/la303360f | Langmuir 2013, 29, 902–912

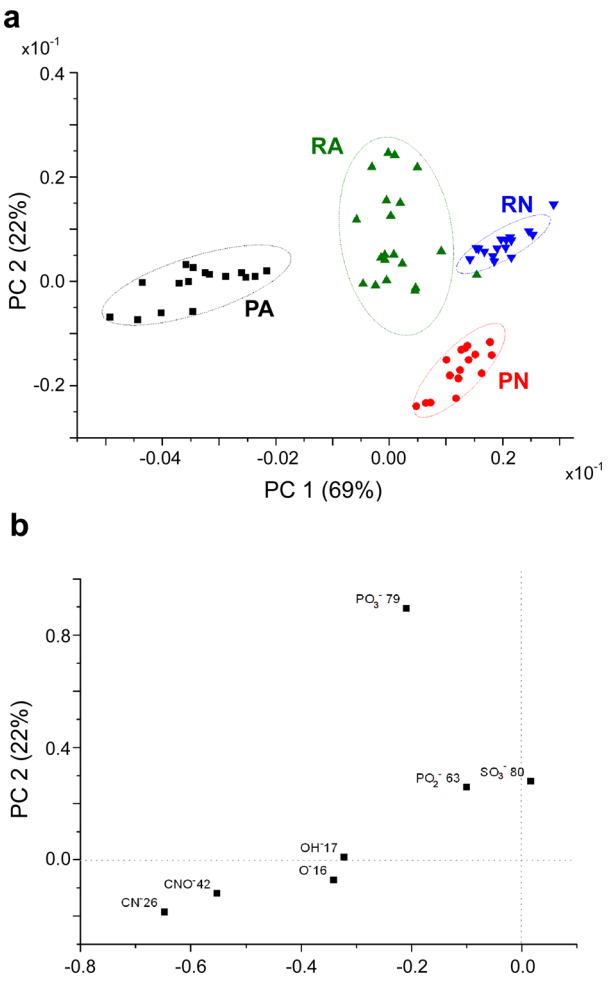

Figure 7. Principal component analysis of the ToF-SIMS data: negative ions. (a) Same as in Figures 5a and 6a, but only the peaks corresponding to the negative ions, which are listed in Table S5 in the Supporting Information, were used. These ions correspond to functional groups and allow the separation of −A samples along PC1 and −N samples along PC2. (b) Loadings plot corresponding to the PCA results shown in part a. The separation is mainly due to functional groups of peptide backbones along PC1 (m/z 26 and 42) and phosphate along PC2 (m/z 79). Residual platelets in PA may explain the similarities of this subset of samples with plasma rich in growth factor samples along PC2 in part a. For clarity, only the high-loading ions are plotted.

related to the peptide backbone on one hand and the sulfide peak on the other (PC1 in Figure 7b). Separation according to the platelet content is accounted for by the phosphate residues (m/z 63 and 79), which load highly in Figure 7b along PC2. As stated above, these are mainly due to the phospholipids present in the plasma rich in growth factors preparations. The negative ion spectra largely confirm the conclusions reached with the positive ion ones.

Lateral Distribution of Chemical Species. ToF-SIMS allows the possibility of mapping the lateral distribution of chemical groups on the surface (imaging). We used the so-called bunched mode to acquire images, where bunching is applied to a pulsed primary ion beam to reduce the pulse width. This mode offers high sensitivity—the number of molecules usable for imaging is almost the limit of the organic secondary ion emission (10^6 molecules/μm^2)—and high mass resolution.[54] These are achieved at the expense of spatial resolution, which in our case is limited to ∼3−5 μm^2. Ions related to the substrate (Table S2 in the Supporting Information) and to amino acids (Table S3 in the Supporting Information) were distributed homogeneously across the sample surfaces in all of the samples; their lateral distribution did not provide further information. On the contrary, the distribution of the phospholipid species (Table S4 in the Supporting Information) in platelet-containing specimens was interesting. Images of the $C_5H_{15}PNO_4^+$ ion (m/z 184, Figure 8a,c,e,g) and PO^{3-} ion (m/z 79, Figure 8b,d,f,h) were selected for their high contrast. Similar results were obtained with several other ions (m/z 30, 72 and 86), but the contrast was lower because of the overlapping protein contributions to these signals (images not shown). In RA samples, round clusters 5 to 20 μm in diameter could be made out (Figure 8a,b) against a rather high, uniform background signal of these species. In the RN samples, well-defined globular entities were visible (Figure 8c,d). These can be reasonably associated with platelets or their aggregates as a result of their size because such clusters were absent in the PN preparations (Figure 8e−h) and because analogous features are visible in the immunofluorescene (Figure 3) and AFM images (Figure 2). Interestingly, although individual platelets could be easily identified in the AFM and immunofluorescence images of both RA and RN preparations, the distribution of the phospholipid-derived ions in the two types of samples was considerably different (cf. Figure 8a,c). Clearly, the difference is related to platelet activation. One of the processes associated with activation is the release of membranous microparticles by platelets.[47] If at least some of them remain associated with the clot, their presence would cause the high background in the phospholipid signal observed.

The residual platelets and their phospholipids present in PA samples are also most likely the reason for the surprising number of phosphates present in PA samples. The images shown in Figure 8 show a systematic difference in the phosphate peak intensity: it is lowest in the PN samples and increases with the platelet content. Once again, better retention of platelets in the activated interfaces (see above) is probably responsible for the difference between PA and PN samples. This rules out the possibility that the phosphate signal arises from the nonspecific phosphate contamination of TiO_2.

CONCLUSIONS

In this study, we used microscopy techniques (SEM, AFM, and immunofluorescence microscopy) together with the combination of time-of-flight secondary ion mass spectrometry (ToF-SIMS) and principal component analysis (PCA) to characterize the morphology and chemical composition of interfaces formed between TiO_2 and four types of blood plasma preparations: plasma rich in growth factors or platelet-poor plasma activated with Ca^{2+} or nonactivated. The most significant finding of our study is that these four types of samples could be distinguished with respect to their chemistry by ToF-SIMS/PCA. Relying on the unique capabilities of this method, we were able to demonstrate that the chemical composition of the protein components of these interfaces was distinct and depended both on whether the platelets were present and on whether the samples were activated with Ca^{2+}. We also showed that a significant fraction of the phospholipid species in the activated, platelet-containing samples was uniformly distributed across the surface, despite the fact that platelet-specific markers are highly localized in the immunofluorescence images. Furthermore, we find a good correlation between sample morphology as

dx.doi.org/10.1021/la303360f | Langmuir 2013, 29, 902−912

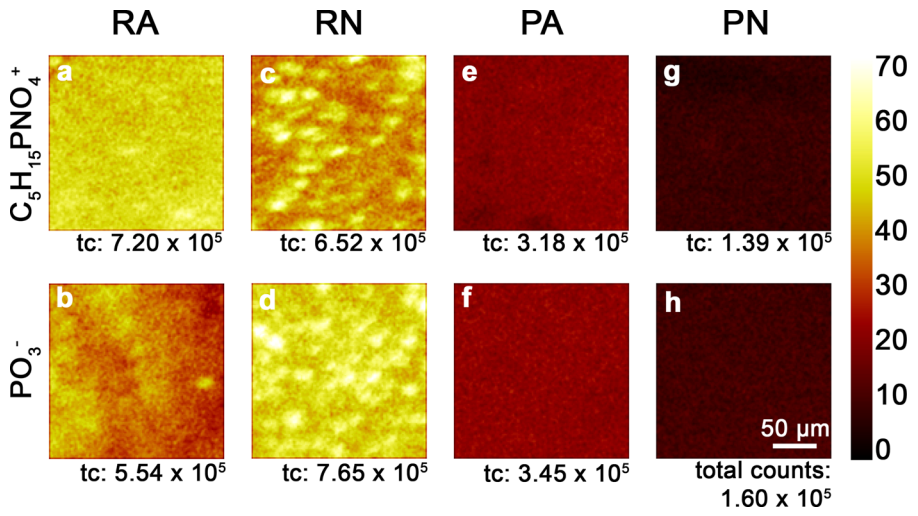

Figure 8. Lateral distribution of phospholipid species in the four types of samples. ToF-SIMS images of the lateral distribution of the chemical groups were recorded for each secondary ion chosen for analysis. All image analysis was performed within the Ion-Tof ion image software (version 6.2, Ion-Tof, GmbH, Munster, Germany). Each image is normalized to the intensity in the brightest pixel (maximum counts per pixel = 70). This intensity value is assigned to the color value of 256. Zero intensity is assigned to the color value of 0. All other intensities are assigned accordingly using a linear relationship. (a, c, e, g) m/z 184 $C_5H_{15}PNO_4^+$; positive phosphatidylcholine headgroup ions. (b, d, f, h) m/z 79 PO_3^-; negative phosphate ions.

identified by SEM and AFM and the accessibility of the substrate (Ti) species as identified by ToF-SIMS. We also find a good correlation between the lateral distribution of phospholipid species as identified in ToF-SIMS images and of platelets as identified by immunofluorescence microscopy in the platelet-containing, nonactivated samples. Our study makes it clear that cells interacting with these interfaces will receive different chemical cues that will different drive their remodeling.

■ ASSOCIATED CONTENT

Supporting Information

XPS analysis of bare substrates and substrates coated with various plasma preparations and compilations of ions used in the various PCA analyses of ToF-SIMS data. This material is available free of charge via the Internet at http://pubs.acs.org

■ AUTHOR INFORMATION

Corresponding Author

*E-mail: ireviakine@cicbiomagune.es. Phone: 34 943 00 53 12. Fax: 34 943 00 53 15.

Notes

The authors declare the following competing financial interest(s): R.T. is employed by and E.A. is the owner and founder of BTI S.L. (Vitoria, Spain), which markets PRGF-Endoret technology for commercial use.

■ ACKNOWLEDGMENTS

We thank the Department of Industry of the Basque Government (grants ETORTEK to I.R. and ETORGAI to E.A., I.R., and others) and the Spanish Ministry of Science and Innovation (MICINN, grant CTQ2009-11245 to I.R.) for funding this project; Dan Graham, Ph.D., for developing the NESAC/BIO Toolbox used in this study and NIH grant EB-002027 used to support the toolbox development; Marcus Textor (ETH-Zürich, Switzerland) for insightful comments and for introducing I.R. to the SIMS facilities at EMPA; María Belén Sánchez-Ilárduya (CIC biomaGUNE) for the XPS analysis of plasma-coated samples; and Michael Horisberger (Paul Scherrer Institut, Villigen, Switzerland) for TiO_2-coated glass coverslips and silicon wafers.

■ REFERENCES

(1) Branemark, P. I. Osseointegration and Its Experimental Background. *J. Prosthet. Dent.* **1983**, *50*, 399−410.
(2) Brunette, D. M.; Tengvall, P.; Textor, M.; Thomsen, P. *Titanium in Medicine*; Springer-Verlag: Berlin, 2001.
(3) Kasemo, B. Biocompatibility of Titanium Implants - Surface Science Aspects. *J. Prosthet. Dent.* **1983**, *49*, 832−837.
(4) Parsegian, V. A. Molecular Forces Governing Tight Contact between Cellular-Surfaces and Substrates. *J. Prosthet. Dent.* **1983**, *49*, 838−842.
(5) Reichert, W. M.; Ratner, B. D.; Anderson, J.; Coury, A.; Hoffman, A. S.; Laurencin, C. T.; Tirrell, D. 2010 Panel on the Biomaterials Grand Challenges. *J. Biomed. Mater. Res. A* **2010**, *96*, 275−287.
(6) Whitman, D. H.; Berry, R. L.; Green, D. M. Platelet Gel: An Autologous Alternative to Fibrin Glue with Applications in Oral and Maxillofacial Surgery. *J. Oral Maxillofac. Surg.* **1997**, *55*, 1294−1299.
(7) Anitua, E. Plasma Rich in Growth Factors: Preliminary Results of Use in the Preparation of Future Sites for Implants. *Int. J. Oral Maxillofac. Implants* **1999**, *14*, 529−535.
(8) Anitua, E.; Sanchez, M.; Orive, G.; Andia, I. The Potential Impact of the Preparation Rich in Growth Factors (PRGF) in Different Medical Fields. *Biomaterials* **2007**, *28*, 4551−4560.
(9) Anitua, E.; Orive, G.; Pla, R.; Roman, P.; Serrano, V.; Andia, I. The Effects of PRGF on Bone Regeneration and on Titanium Implant Osseointegration in Goats: A Histologic and Histomorphometric Study. *J. Biomed. Mater. Res. A* **2009**, *91*, 158−165.
(10) Anitua, E.; Sanchez, M.; Prado, R.; Orive, G. Plasma Rich in Growth Factors: The Pioneering Autologous Technology for Tissue Regeneration. *J. Biomed. Mater. Res. A* **2011**, *97*, 536.
(11) Eppley, B. L.; Pietrzak, W. S.; Blanton, M. Platelet-Rich Plasma: A Review of Biology and Applications in Plastic Surgery. *Plast. Reconstr. Surg.* **2006**, *118*, 147E−159E.
(12) Lieberman, J. R.; Daluiski, A.; Einhorn, T. A. The Role of Growth Factors in the Repair of Bone. Biology and Clinical Applications. *J. Bone Joint Surg. Am.* **2002**, *84A*, 1032−44.
(13) Slapnicka, J.; Fassmann, A.; Strasak, L.; Augustin, P.; Vanek, J. Effects of Activated and Nonactivated Platelet-Rich Plasma on

Proliferation of Human Osteoblasts in Vitro. *J. Oral Maxillofac. Surg.* **2008**, *66*, 297−301.
(14) Kark, L. R.; Karp, J. M.; Davies, J. E. Platelet Releasate Increases the Proliferation and Migration of Bone Marrow-Derived Cells Cultured under Osteogenic Conditions. *Clin. Oral Implants Res.* **2006**, *17*, 321−327.
(15) Kanno, T.; Takahashi, T.; Tsujisawa, T.; Ariyoshi, W.; Nishihara, T. Platelet-Rich Plasma Enhances Human Osteoblast-like Cell Proliferation and Differentiation. *J. Oral Maxillofac. Surg.* **2005**, *63*, 362−369.
(16) Torres, J.; Tamimi, F.; Martinez, P. P.; Alkhraisat, M. H.; Linares, R.; Hernandez, G.; Torres-Macho, J.; Lopez-Cabarcos, E. Effect of Platelet-Rich Plasma on Sinus Lifting: A Randomized-Controlled Clinical Trial. *J. Clin. Periodontol.* **2009**, *36*, 677−687.
(17) Anitua, E. A. Enhancement of Osseointegration by Generating a Dynamic Implant Surface. *J. Oral Implantol.* **2006**, *32*, 72−76.
(18) Fontana, S.; Olmedo, D. G.; Linares, J. A.; Guglielmotti, M. B.; Crosa, M. E. Effect of Platelet-Rich Plasma on the Peri-Implant Bone Response: An Experimental Study. *Implant Dent.* **2004**, *13*, 73−78.
(19) Zechner, W.; Tangl, S.; Tepper, G.; Furst, G.; Bernhart, T.; Haas, R.; Mailath, G.; Watzek, G. Influence of Platelet-Rich Plasma on Osseous Healing of Dental Implants: A Histologic and Histomorphometric Study in Minipigs. *Int. J. Oral Maxillofac. Implants* **2003**, *18*, 15−22.
(20) Anitua, E.; Alkhraisat, M. H.; Orive, G. Perspectives and Challenges in Regenerative Medicine Using Plasma Rich in Growth Factors. *J. Controlled Release* **2012**, *10*, 29−38.
(21) Sánchez-Ilárduya, B. M.; Trouche, E.; Tejero, R.; Reviakine, I.; Anitua, E. Time-Dependent Release of Growth Factors from Implant Surfaces Treated with Blood Plasma Preparations: Effects of Platelet Concentration and Activation Procedure. *J. Biomed. Mater. Res. A* **2012**, accepted for publication.
(22) Michel, R.; Castner, D. G. Advances in Time-of-Flight Secondary Ion Mass Spectrometry Analysis of Protein Films. *Surf. Interface Anal.* **2006**, *38*, 1386−1392.
(23) Wagner, M. S.; Castner, D. G. Characterization of Adsorbed Protein Films by Time-of-Flight Secondary Ion Mass Spectrometry with Principal Component Analysis. *Langmuir* **2001**, *17*, 4649−4660.
(24) Chatterjee, R. Application of TOF-SIMS to Monitor Coating Processes on Biological and Organic Surfaces. *Appl. Surf. Sci.* **2004**, *231*, 437−441.
(25) Belu, A. M.; Graham, D. J.; Castner, D. G. Time-of-Flight Secondary Ion Mass Spectrometry: Techniques and Applications for the Characterization of Biomaterial Surfaces. *Biomaterials* **2003**, *24*, 3635−3653.
(26) Lhoest, J. B.; Wagner, M. S.; Tidwell, C. D.; Castner, D. G. Characterization of Adsorbed Protein Films by Time of Flight Secondary Ion Mass Spectrometry. *J. Biomed. Mater. Res.* **2001**, *57*, 432−440.
(27) Tidwell, C. D.; Castner, D. G.; Golledge, S. L.; Ratner, B. D.; Meyer, K.; Hagenhoff, B.; Benninghoven, A. Static Time-of-Flight Secondary Ion Mass Spectrometry and X-ray Photoelectron Spectroscopy Characterization of Adsorbed Albumin and Fibronectin Films. *Surf. Interface Anal.* **2001**, *31*, 724−733.
(28) Canavan, H. E.; Graham, D. J.; Cheng, X. H.; Ratner, B. D.; Castner, D. G. Comparison of Native Extracellular Matrix with Adsorbed Protein Films Using Secondary Ion Mass Spectrometry. *Langmuir* **2007**, *23*, 50−56.
(29) Wagner, M. S.; Castner, D. G. Analysis of Adsorbed Proteins by Static Time-of-Flight Secondary Ion Mass Spectrometry. *Appl. Surf. Sci.* **2004**, *231*, 366−376.
(30) Xia, N.; May, C. J.; McArthur, S. L.; Castner, D. G. Time-of-Flight Secondary Ion Mass Spectrometry Analysis of Conformational Changes in Adsorbed Protein Films. *Langmuir* **2002**, *18*, 4090−4097.
(31) Vaezian, B.; Anderton, C. R.; Kraft, M. L. Discriminating and Imaging Different Phosphatidylcholine Species within Phase-Separated Model Membranes by Principal Component Analysis of TOF-Secondary Ion Mass Spectrometry Images. *Anal. Chem.* **2010**, *82*, 10006−10014.
(32) Vaidyanathan, S.; Fletcher, J. S.; Goodacre, R.; Lockyer, N. P.; Micklefield, J.; Vickerman, J. C. Subsurface Biomolecular Imaging of *Streptomyces coelicolor* Using Secondary Ion Mass Spectrometry. *Anal. Chem.* **2008**, *80*, 1942−1951.
(33) Wagner, M. S.; Horbett, T. A.; Castner, D. G. Characterizing Multicomponent Adsorbed Protein Films Using Electron Spectroscopy for Chemical Analysis, Time-of-Flight Secondary Ion Mass Spectrometry, And Radiolabeling: Capabilities and Limitations. *Biomaterials* **2003**, *24*, 1897−1908.
(34) Kurrat, R.; Textor, M.; Ramsden, J. J.; Boni, P.; Spencer, N. D. Instrumental Improvements in Optical Waveguide Light Mode Spectroscopy for the Study of Biomolecule Adsorption. *Rev. Sci. Instrum.* **1997**, *68*, 2172−2176.
(35) Sittig, C. E. Charakterisierung der Oxidschichten auf Titan und Titanlegierungen sowie deren Reaktionen in Kontakt mit Biologisch Relevanten Modellösungen. Ph.D. Thesis, ETH Zurich: Zurich, Switzerland, 1998.
(36) Textor, M.; Sittig, C.; Frauchiger, V.; Tosatti, S.; Brunette, D. M., Properties and Biological Significance of Natural Oxide Films on Titanium and Its Alloys. In *Titanium in Medicine*; Brunette, D. M., Tengvall, P., Textor, M., Thomsen, P., Eds.; Springer-Verlag: Berlin, 2001; pp 172−224.
(37) Callen, B. W.; Lowenberg, B. F.; Lugowski, S.; Sodhi, R. N.; Davies, J. E. Nitric Acid Passivation of Ti6Al4V Reduces Thickness of Surface Oxide Layer and Increases Trace Element Release. *J. Biomed. Mater. Res.* **1995**, *29*, 279−290.
(38) Green, F. M.; Gilmore, I. S.; Seah, M. P. TOF-SIMS: Accurate Mass Scale Calibration. *J. Am. Soc. Mass Spectrom.* **2006**, *17*, 514−523.
(39) Mantus, D. S.; Ratner, B. D.; Carlson, B. A.; Moulder, J. F. Static Secondary-Ion Mass-Spectrometry of Adsorbed Proteins. *Anal. Chem.* **1993**, *65*, 1431−1438.
(40) Asakawa, D.; Yoshimura, K.; Takeda, S.; Hiraoka, K. Direct Analysis of Lipids in Mouse Brain Using Electrospray Droplet Impact/SIM. *J. Mass Spectrom.* **2010**, *45*, 437−443.
(41) Nygren, H.; Borner, K.; Hagenhoff, B.; Malmberg, P.; Mansson, J. E. Localization of Cholesterol, Phosphocholine and Galactosylceramide in Rat Cerebellar Cortex with Imaging TOF-SIMS Equipped with a Bismuth Cluster Ion Source. *Biochim. Biophys. Acta, Mol. Cell Biol. Lipids* **2005**, *1737*, 102−110.
(42) NESAC/BIO MVA website: http://mvsa.nb.uw.edu.
(43) Goldstein, J. I.; Newbury, D. E.; Echlin, P.; Joy, D. C.; Fiori, C.; Lifshin, E. *Scanning Electron Microscopy and X-ray Microanalysis*; Plenum Press: New York, 1992.
(44) Bozzola, J. J.; Russell, L. D. *Electron Microscopy Principles and Techniques for Biologists*; Jones and Bartlett Publishers: Sudbury, MA, 1999.
(45) Dykstra, M. J. *Biological Electron Microscopy Theory, Techniques, and Troubleshooting*; Plenum Press: New York, 1992.
(46) Pretorius, E.; Humphries, P.; Ekpo, O. E.; Smit, E.; Van Der Merwe, C. F. Comparative Ultrastructural Analyses of Mouse, Rabbit, And Human Platelets and Fibrin Networks. *Microsc. Res. Tech.* **2007**, *70*, 823−827.
(47) Michelson, A. *Platelets*, 2nd ed.; Academic Press: London, 2007.
(48) Lam, W. A.; Chaudhuri, O.; Crow, A.; Webster, K. D.; Li, T. D.; Kita, A.; Huang, J.; Fletcher, D. A. Mechanics and Contraction Dynamics of Single Platelets and Implications for Clot Stiffening. *Nat. Mater.* **2011**, *10*, 61−66.
(49) Dellinger, M.; Geze, M.; Santus, R.; Kohen, E.; Kohen, C.; Hirschberg, J. G.; Monti, M. Imaging of Cells by Autofluorescence: A New Tool in the Probing of Biopharmaceutical Effects at the Intracellular Level. *Biotechnol. Appl. Biochem.* **1998**, *28*, 25−32.
(50) Ryan, E. A.; Mockros, L. F.; Weisel, J. W.; Lorand, L. Structural Origins of Fibrin Clot Rheology. *Biophys. J.* **1999**, *77*, 2813−26.
(51) Garrison, B. J.; Postawa, Z. Computational View of Surface Based Organic Mass Spectrometry. *Mass Spectrom. Rev.* **2008**, *27*, 289−315.
(52) Coppinger, J. A.; Cagney, G.; Toomey, S.; Kislinger, T.; Belton, O.; McRedmond, J. P.; Cahill, D. J.; Emili, A.; Fitzgerald, D. J.; Maguire, P. B. Characterization of the Proteins Released from

Activated Platelets Leads to Localization of Novel Platelet Proteins in Human Atherosclerotic Lesions. *Blood* **2004**, *103*, 2096−104.
(53) Claeys, D.; Geering, K.; Meyer, B. J. Two-Dimensional Blue Native/Sodium Dodecyl Sulfate Gel Electrophoresis for Analysis of Multimeric Proteins in Platelets. *Electrophoresis* **2005**, *26*, 1189−99.
(54) Hoshi, T.; Kudo, M. High Resolution Static SIMS Imaging by Time of Flight SIMS. *Appl. Surf. Sci.* **2003**, *203*, 818−824.
(55) Chen, F. M.; Zhang, J.; Zhang, M.; An, Y.; Chen, F.; Wu, Z. F. A Review on Endogenous Regenerative Technology in Periodontal Regenerative Medicine. *Biomaterials* **2010**, *31*, 7892−927.